CHAPTER 2

ANALYSIS OF GYROKLYSTRON AMPLIFIERS*

2.1 Introduction
2.2 Nonlinear Analysis
  2.2.1 Effect of the beam velocity spread
  2.2.2 Linear analysis
2.3 Results and Discussion
  2.3.1 Efficiency contours
  2.3.2 Numerical benchmarking
    2.3.2.a Two-cavity gyroklystron amplifier
    2.3.2.b Four-cavity gyroklystron amplifier
  2.3.3 Sensitivity analysis
2.4 Conclusion

*Part of this work has been published as

1. **M. S. Chauhan,** M. V. Swati and P. K. Jain, "Estimation of the electronic efficiency of a gyroklystron amplifier," *International Journal of Microwaves Applications*, Vol. 2, No. 1, pp. 23-27, 2013.
2. **M. S. Chauhan,** and P. K. Jain, "Electron Bunching in the Gyroklystron Amplifiers," *International Journal on Advanced Circuits and Systems.* (Accepted)

2.1 Introduction

In recent years, there are renewed interest and activities in developing gyro-devices, like, gyrotrons, gyro TWTs, gyroklystrons, etc., which belong to the fast-wave microwave electron beam device family. These fast wave devices utilize a periodic gyrating electron beam in a smooth wall interaction structure supporting a fast waveguide mode. The operating principle of such a device is based on the electron cyclotron resonance maser (ECRM) instability that allows for large transverse dimensions of the interaction structure, operation at higher harmonics of the waveguide and beam cyclotron harmonic modes making the generation or amplification to produce high powers even at millimeter wavelengths using reasonable values of background magnetic fields. Amongst all the gyro-devices, gyrotron, which is a fixed frequency high power oscillator in the millimeter and sub-millimeter waves range, has been matured both analytically and experimentally during the last few decades primarily due to its variety of applications. Consequently, the various relevant concepts of other gyro-devices, like, gyroklystrons, gyroTWTs, gyrotwystrons have been derived from those of gyrotrons [Flyagin *et al.* (1988), Granatstein *et al.* (1983), Symons *et al.* (1986)].

Gyroklystron, an amplifier of this family, is emerged as a promising candidate due to its capability to provide high gain and moderate bandwidth with good linearity and phase stability in the millimeter and sub-millimeter wave regime [Barker *et al.* (2001), Nusinovich (2004)]. In the family of gyro-devices, gyroklystron amplifiers are still at the development stage and have not reached to the status of a matured device in the manufacturer product range.

Analytical research led to the considerable physical insight into the principle of operation of the gyroklystrons. There are primarily two analytical approaches used for modeling of the gyroklystron amplifiers as reported by different authors [Tran *et al.* (1986), Salop *et al.* (1986), Geng *et al.* (2004), Nusinovich (2004), Luo *et al.* (2005), Wang *et al.* (2008), Jianhua *et al.* (2011), Shou-Xi *et al.* (2012)]. In the first approach, a fixed profile function is used to describe the RF field in the cavities of gyroklystrons, i. e., the effect of the electron beam on the RF profile is neglected. The second approach is based on

the self-consistent theory where the equations of motion for the electrons are solved simultaneously with the help of the field equations, taking into account the effect of the electron beam on cavity field profile, instead of using a fixed field profile. These models are basically derived using the work reported by Fliflet *et al*. for analyzing the gyrotron oscillators [Fliflet *et al.* (1982)]. However, the methods adopted for numerical solution of the equations to compute the efficiency of the gyroklystron are different. These methods include time independent and time dependent analysis.

Some of the reported analytical work for investigating the gyroklystron beam-wave interaction behavior are: the development of the generalized time independent single mode analysis considering the fixed RF profiles based on the linear and nonlinear analyses, point gap model [Tran *et al.* (1986), Nusinovich (2004)], and development of large signal codes for gyroklystron amplifier using the self-consistent calculation [Salop *et al.* (1986), Geng *et al.* (2004), Luo *et al.* (2005), Wang *et al.* (2008), Jianhua *et al.* (2011), Shou-Xi *et al.* (2012)]. These gyroklystron models are restricted using certain assumptions, i.e., ignoring space charge effects, complete isolation between the RF cavities, uniform guiding magnetic field to make the analysis simpler and to reduce the computation time. The effects of velocity spread are also not taken into considerations while carrying out the analysis [Tran *et al.* (1986), Geng *et al.* (2004), Nusinovich (2004), Luo *et al.* (2005), Wang *et al.* (2008), Jianhua *et al.* (2011)] whereas included by [Salop *et al.* (1986)], and [Shou-Xi *et al*. (2012)]. In most of the reported literature on gyroklystrons, the single mode operation is considered in each cavity except in [Luo *et al.* (2005)] where a semi-multimode approach is used to analyze the beam-wave interaction behavior in the operating mode as well as the other modes with the same azimuthal index but different radial indices.

In the earlier reported work of single mode gyroklystron analysis [Tran *et al.* (1986)], the results are presented in terms of normalized parameters through graphical analysis based on contour plots [Tran *et al.* (1986)] which has been extended and reported here in this chapter is in terms of the mathematical model. Since, it is rather difficult to optimise the performance of a gyroklystron amplifier

using this approach through the graphical interpretation of the contour plots. Therefore, in the present Chapter 2, this analysis for gyro-devices based on the contour plots has been extended to analyze the gyroklystron amplifiers in terms of computer friendly mathematical model. In [Tran *et al.* (1986)] the equations of motion are solved only for the output cavity of the gyroklystron to optimize the orbital efficiency of the device by arbitrarily choosing the normalized parameters of specific range. Thus, [Tran *et al.* (1986)] does not provide the comprehensive scenario of the amplification process taking place in each stage of the device as one moves from the input cavity to output cavity. Furthermore, the variation of efficiency with frequency is not carried out in [Tran *et al.* (1986)] to estimate the bandwidth of the device. Therefore, in the present Chapter 2, the equations of motion have been solved for each cavity of the gyroklystron amplifier by considering actual parameters of the device instead of arbitrarily chosen parameters to estimate the efficiency in each cavity. The bandwidth of the device is estimated by studying the effect of frequency variations on RF output power. Moreover, the effects of electron beam velocity spread on the performance of gyroklystron amplifier are considered in the present model, which were not taken into account in [Tran *et al.* (1986)].

For the benchmarking of the developed mathematical model, the performance evaluation of the typical selected 35 GHz two-cavity and four-cavity experimental gyroklystron amplifiers have been carried out and validated against the reported experimental results in the literature. The mathematical model developed here will be used in developing the design methodology and performance improvements techniques for the gyroklystron amplifiers in the subsequent chapters.

2.2 Nonlinear Analysis

The nonlinear analysis is used to study the evolution of the electron beam in the background of electromagnetic wave supported by the interaction structure and a static axial magnetic field. The nonlinear theory presented here is more general and advantageous in many ways. One of the features of the present

analysis lies in its validity for all the gyroklystrons operating at arbitrary cyclotron harmonics and any waveguide mode. It is important to maintain synchronism between external magnetic field and the gyrating electrons to enhance the interaction efficiency. This goal can be achieved by tapering of the external magnetic field [Nusinovich (1992)]. The non-uniformity of background magnetic field can also be implemented in the present theory. This is a full nonlinear description of the interaction process that too depicts the device saturation effect.

The analysis starts with the Maxwell's equation leading to express field components of a circular cylindrical waveguide excited in the TE_{mn} mode. In order to include the effect of the electron beam, a source present term in the wave equation is considered. Further, in order to obtain the wave equation in terms of the slow time scale variables, the transformation of the coordinates from the cylindrical system to guiding center system is required. Graf's summation theorem for Bessel's functions has been used to incorporate this transformation [Winternitz *et al*. (2001), Basu (1996)]. Finally, the circuit equations govern the evolution of amplitude and phase of electromagnetic fields. The electron beam dynamics, which govern the motion of the RF wave and electrons in the presence of a static axial magnetic field (assuming the space charge fields to be negligible), is explained with the help of relativistic Lorentz force equation for an electron interacting with a TE_{mn} waveguide mode.

In the present approach, certain assumptions are made. The space-charge effects on the electron beam are ignored. Here, in this nonlinear theory, it is assumed that all the electrons have the same kinetic energy. A quasi-static system is assumed in the sense that the particles, entering the interaction region separated by integral multiples of a wave period, will travel along similar trajectories. With this assumption, the slow-time scale formalism can be followed where fast scale phenomena such as the electron cyclotron motion, and the sinusoidal variations of the RF field are eliminated through averaging over a period while the more important slow-time scale spatial variations of the fields are retained. In this procedure, the dynamics of a single wave is determined in terms of ensemble average over the nonlinear electron trajectories. The misalignment effect can be

observed using the nonlinear analysis by assuming the change in the initial distribution of guiding centers of the particles.

Since, gyroklystron operates in circular transverse electric (TE_{mn}) modes (similar to gyrotron) near cutoff, i.e., $\omega/c = k = \left(k_\perp + k_\parallel\right)^{1/2}$ with $k_\perp >> k_\parallel$, where ω is the RF angular frequency, c is the velocity of light, $k_\perp$ and $k_\parallel$ are the transverse and axial wave numbers, respectively, of the waveguide modes. In this case, we take $\omega/c = k \approx k_\perp = \nu_{mn}/r_w$ for TE_{mn} modes, where r_w is the cavity radius and ν_{mn} is the n^{th} zero of Bessel function $J'_m(x)$. The combination of this condition and cyclotron condition, $\omega = s\omega_c$ determine the operating mode of a gyroklystron. Here, $\omega_c = eB_0/\gamma m_e$ is the relativistic electron cyclotron frequency, s is the harmonic number, m_e is the electron rest mass, B_0 is the DC magnetic field, and γ is the relativistic factor. The gyroklystron interaction results from phase bunching of electrons by an RF field due to the energy dependence of their cyclotron frequency.

The generalized nonlinear theory for a harmonic gyroklystron can be developed in the form of generalized pendulum equations used for the gyrotrons, as the RF interaction structure of a gyroklystron is quite similar to a gyrotron. The equations of motions for an electron moving in combined electric and magnetic fields in terms of energy $\varepsilon (= \gamma m_e c^2)$ and momentum $\left(|p| = \gamma\beta m_e c\right)$ can be given as:

$$\frac{d\varepsilon}{dt} = -ev \cdot E \quad , \tag{2.1}$$

$$\frac{dp}{dt} = -ev - \frac{e}{c} v \times B \quad , \tag{2.2}$$

where, e, v, E, and $\gamma = \left(1 - \beta_\perp^2 - \beta_\parallel^2\right)^{-1/2}$ are the electronic charge, electron velocity, electric field, and relativistic mass factor, respectively. $\beta_\perp (= v_\perp/c)$ and $\beta_\parallel (= v_\parallel/c)$ are the normalized electron velocities in transverse and axial directions, respectively. In the present theory, a fixed axial profile of the electromagnetic field is assumed but in the azimuthal direction, it is rotating. This assumption is

valid when the source term in the Maxwell's equation is negligible, i.e., the effect of presence of an electron beam does not alter significantly the field profile. For a high quality factor gyrotron and gyroklystron, this approximation is reasonable. The effect of the RF magnetic field on the electron motion is ignored provided that the phase velocity of RF field is much greater than the speed of light that obtained for a wave near cutoff. The magnetic field is taken to be the axial static guide field $B = B_0 \hat{z}$. The energy variable (ε) can be written in terms of a relative energy variable (w) using Einstein's mass-energy equivalence relation and axial dependence can be transformed as:

$$w = \frac{\gamma_0 m_e c^2 - \gamma m_e c^2}{\gamma_0 m_e c^2} = 1 - \gamma/\gamma_0 \text{, and } Z = \left(\omega / c\beta_{\|0}\right) z \tag{2.3}$$

respectively. Here (γ_0) is the initial value of relativistic factor and (γ) is the final value of relativistic factor. Therefore, equation (2.1) can be transformed as:

$$\frac{dw}{dZ} = \frac{e}{(m_e c)^2 \omega} \frac{\beta_{\|0}}{\gamma \gamma_0 \beta_{\|}} pE \quad , \tag{2.4}$$

where, $\beta_{\|0}$ and γ_0 are the values of $\beta_{\|}$ and γ at the input of the interaction structure, respectively. In the complex notation, p and E can be written as

$$p = p_x + ip_y = |p_+|\cos\zeta + i|p_+|\sin\zeta = |p_+|e^{i\zeta} \quad ,$$

$$E = E_x + iE_y = |E_+|\cos(\omega t + \psi) + i|E_+|\sin(\omega t + \psi) = |E_+|e^{i(\omega t + \psi)} \quad ,$$

where, ζ is the angle of the electron momentum vector about the gyro-center (Fig. 2.1). The electron gyro-center is located at a radius r_b from the cavity center. Now,

$$\begin{aligned} p.E = p_x E_x + p_y E_y &= |p_+||E_+|(\cos\zeta\cos(\omega t + \psi) + \sin\zeta\sin(\omega t + \psi)) \\ &= |p_+||E_+|\cos(\zeta - (\omega t + \psi)) = \mathrm{Re}(p_+^* E_+) \quad . \end{aligned} \tag{2.5}$$

Using (2.5), (2.4) can be expressed as

$$\frac{dw}{dZ} = \frac{e}{(m_e c)^2 \omega} \frac{\beta_{\|0}}{\gamma \gamma_0 \beta_{\|}} \mathrm{Re}(p_+^* E_+) \quad . \tag{2.6}$$

Similarly, for the phase of the electron can be written from (2.2) as:

$$\frac{d\zeta}{dZ} = \frac{\beta_{\|0}\omega_c}{\beta_{\|}\omega} - \frac{e\beta_{\|0}}{\beta_{\|}\omega|p_+|} \mathrm{Im}(p_+^* E_+) \quad . \tag{2.7}$$

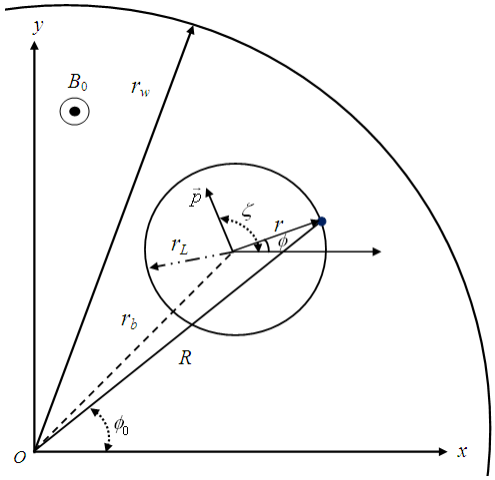

Fig. 2.1 Arrangement of gyrating electrons in their Larmor radius in the cylindrical cavity with cartesian and cylindrical coordinate systems.

Here, $\omega_c = eB_0/(\gamma m_e)$ is the cyclotron frequency. In the Fig. 2.1, the coordinate of an electron gyrating along the cavity center at a beam radius r_b. Here, r_L, r_w, and R are the Larmor radius, cavity radius and the position of electron in the cavity center respectively. The electric field for a TE_{mn} mode near cutoff in a circular cross-section can be written in the cylindrical coordinate system (R, ϕ_0) with origin at the center of the cavity (Fig. 2.1) as:

$$E = (E_r \hat{R} + E_{\varphi_0} \hat{\varphi}_0) e^{i(\omega t + \psi)}, \tag{2.8}$$

$$E_R = i\left(\frac{m}{k_\perp R}\right) E_0 f(z) J_m(k_\perp R) e^{-im\varphi_0}, \tag{2.9}$$

$$E_{\varphi_0} = E_0 f(z) J'_m(k_t R) e^{-im\varphi_0}. \tag{2.10}$$

The field used here is that of a rotating mode, E_0 is the field amplitude, and $f(z)$ is the normalized axial field profile of unit amplitude. Now, using the Graf's summation theorem for Bessel functions, the electric field in the (R, ϕ_0) coordinate system can be transformed to (r, ϕ) coordinate system centered at electron gyro-center to obtain the synchronism condition ($\omega \approx s\omega_c$) [Basu (1996)]. Hence, the component of the RF field for the s^{th} order cyclotron resonance can be written as:

$$E = (E_{rs} \hat{r} + E_{\phi s} \hat{\phi}) e^{i(\omega t + \psi)} \tag{2.11}$$

$$E_{rs} = i(\frac{s}{k_\perp r})E_0 f(z) J_{m\pm s}(k_\perp r_b) J_s(k_\perp r) e^{-im\varphi_0} e^{-is(\varphi-\varphi_0)} \tag{2.12}$$

$$E_{\varphi s} = E_0 f(z) J_{m\pm s}(k_\perp r_b) J'_s(k_\perp r) e^{-im\varphi_0} e^{-is(\varphi-\varphi_0)} . \tag{2.13}$$

The electric field of a TE_{mn} cavity mode can be then expressed as:

$$E_+ = -E_r \sin[\theta + \psi - (m-s)\varphi_0] e^{i\varphi} + iE_\varphi \cos[\theta + \psi - (m-s)\varphi_0] e^{i\varphi} \tag{2.14}$$

where, E_r and E_ϕ are defined as $E_r = |E_{rs}|$ and $E_\phi = |E_{\phi s}|$. The slow-time scale phase variable $\theta = \omega t - s\varphi$ has been introduced and ζ to be transformed into θ in the equation (2.7). The angle of electron momentum ζ is related with electron phase ϕ as $\zeta = \phi + \pi/2$. Using (2.14), (2.6) and (2.7) can be written as:

$$\frac{dw}{dZ} = \frac{e}{m_e c\omega\gamma_0} p'_\perp E_\varphi \cos(\theta + \psi - (m-s)\varphi_0) \tag{2.15}$$

$$\frac{d\theta}{dZ} = \delta_0 - w - \frac{en}{m_e c\omega\gamma_0}\frac{(1-w)}{p'_\perp} E_r \sin[\theta + \psi - (m-s)\varphi_0] \quad , \tag{2.16}$$

where, $p'_\perp = |p_+| / (m_e c\gamma_0) = (\beta^2_{\perp 0} - 2w + w^2)^{1/2}$ and $\delta_0 = 1 - s\,\omega_{c0}/\omega$ is the magnetic field detuning parameter where, $\omega_{c0} = eB_0 / (\gamma_0 m_e)$. In the gyrotrons, there is no bunching of the electron beam at the entrance to the cavity, therefore, choice of RF phase ψ can be arbitrary. In general, ψ can be expressed in terms of the axial dependence *Z*, it is assumed to be constant throughout the interaction region by taking as $\psi - (m-s)\phi_0 = -\pi/2$ and setting $\omega \approx s\omega_{c0}$. Hence, (2.15) and (2.16) can be written as:

$$\frac{dw}{dZ} = \frac{E_\varphi}{sB_0} p'_\perp \sin\theta \quad , \tag{2.17}$$

$$\frac{d\theta}{dZ} = \delta_0 - w - \frac{E_r}{B_0}\frac{(1-w)}{p'_\perp}\cos\theta \quad . \tag{2.18}$$

Equation (2.17) represents the inertial bunching of electrons due to the effect of azimuthal electric field which results a modulation in energy distribution of electrons. Further, the phase variation occurs due to radial electric field and the inertial bunching. The argument of the Bessel function J_s of the electric field can be written in terms of energy variable as:

$$k_\perp r \approx \frac{w}{c} r \approx \frac{s\gamma\beta_\perp}{\gamma_0} = s\beta_{\perp 0}[1-\frac{1}{{\beta_{\perp 0}}^2}(2w-w^2)]^{\frac{1}{2}} = sp'_\perp \quad , \tag{2.18a}$$

Now, introducing the energy and axial position variable as:

$$u = \frac{2}{{\beta_{\perp 0}}^2} w = \frac{2}{{\beta_{\perp 0}}^2}(1-\frac{\gamma}{\gamma_0}) \quad , \qquad \varsigma = \frac{{\beta_{\perp 0}}^2}{2} Z = \pi \frac{{\beta_{\perp 0}}^2}{\beta_{\|0}} \frac{z}{\lambda} \quad . \tag{2.18b}$$

The equations (2.17) and (2.18) can be written as:

$$\frac{du}{d\varsigma} = 2(\frac{s!2^s}{s^s {\beta_{\perp 0}}^{s-1}}) Ff(\varsigma) \frac{p'_\perp}{\beta_{\perp 0}} J'_s(sp'_\perp)\sin\theta \tag{2.19}$$

$$\frac{d\theta}{d\varsigma} = \Delta - u - s(\frac{s!2^s}{s^s {\beta_{\perp 0}}^{s-1}}) Ff(\varsigma) \frac{\beta_{\perp 0}(1-{\beta_{\perp 0}}^2 u/2)}{p'^2_t} J_s(sp'_\perp)\cos\theta \quad , \tag{2.20}$$

where, the normalized field amplitude (F), normalized length (μ) and the detuning parameter (Δ) are defined as

$$F = \frac{E_0}{B_0 c} {\beta_{\perp 0}}^{s-4} \left(\frac{s^{s-1}}{s!2^{s-1}} \right) J_{m\pm s}(k_\perp r_b) \, , \tag{2.20a}$$

$$\mu = \pi \frac{{\beta_{\perp 0}}^2}{\beta_{\|0}} \frac{L}{\lambda} \quad , \tag{2.20b}$$

$$\Delta = \frac{2\delta_0}{\beta_{\perp 0}^2} = \frac{2}{\beta_{\perp 0}^2}\left(1 - s\,\omega_{c0}/\omega\right) \quad . \tag{2.20c}$$

The plus and minus sign in the Bessel function subscript denotes the counter and co-rotating mode of rotation of the RF field. The electric field amplitude E_0 can be calculated as $E_0 = \sqrt{\frac{QP_{in}}{\omega\varepsilon_0\pi L}} \frac{2}{R_w \mid J_m(\nu_{mn}) \mid}$ [Joye *et al.* (2004)]. Here Q is the total quality factor of the cavity, P_{in} is the driver power, L is the length of cavity and r_w is the cavity wall radius. The three important parameters have been introduced, and the equation of motions will finally be expressed in terms of these parameters. Under the condition of weakly relativistic electron beam and the condition

$$s\beta_{\perp 0}^2/2 \ll 1 \quad , \tag{2.21}$$

is satisfied, then $p'_\perp$ can be approximated as $p'_\perp \approx \left({\beta_{\perp 0}}^2 - 2\omega\right)^{1/2} = \beta_{\perp 0}\left(1-u\right)^{1/2}$. Under the condition given by (2.21), Bessel function $J_s(sp'_\perp)$ can be approximated as:

$$J_m(x) = \frac{1}{m!}\left(\frac{x}{2}\right)^m, \quad x << 1, m \neq 0$$

$$= 1 - \frac{1}{4}(x)^2, \quad x << 1, \quad m = 0 .$$

Then, equations (2.19) and (2.20) can be expressed in terms of normalized parameters F, μ, and Δ as

$$\frac{du}{d\varsigma} = 2Ff(\varsigma)(1-u)^{1/2}\sin\theta \tag{2.22}$$

$$\frac{d\theta}{d\varsigma} = \Delta - u - sF\, f(\varsigma)(1-u)^{(s/2)-1}\cos\theta \tag{2.23}$$

Also, the normalized momentum (p) of electrons can be expressed in terms of their normalized energy (u) as [Nusinovich (2004)]:

$$u = 1 - \frac{p_\perp^2}{p_{\perp 0}^2} = 1 - p^2 \quad . \tag{2.24}$$

Now, after differentiating equation (2.24) with respect to ς and using equation (2.24) in equations (2.22) and (2.23) we get

$$\frac{dp}{d\varsigma} = -Ff(\varsigma)(p)^{s-1}\sin(\theta) \quad , \tag{2.25}$$

$$\frac{d\theta}{d\varsigma} = (\Delta + p^2 - 1) - sFf(\varsigma)(p)^{s-2}\cos(\theta) \quad . \tag{2.26}$$

These are the two nonlinear pendulum equations which describe the interaction of an electron beam with the cavity RF field of a gyrotron and a gyroklystron amplifier with $p(\varsigma_{in}) = 1$ and $\theta(\varsigma_{in}) = \theta_0$, where θ_0 is uniformly distributed all over the phase (0, 2π) and where p, θ, F, Δ and ς are the normalized momentum, electron phase, normalized field amplitude, frequency detuning parameter and normalized axial position respectively. In the equations (2.25) and (2.26) $f(\varsigma)$ is the axial field profile which is approximated by Gaussian function for most of the cases and is given by:

$$f(\varsigma) = \exp\left(-(2\varsigma/\mu)^2\right) \text{ or } f(z) = \exp\left(-(2z/L)^2\right) , \tag{2.27}$$

where, L is the length of the cavity.

In devices like gyrotrons and gyroklystrons the maximum energy transfer occurs when the electron cyclotron motion is approximately in synchronism with the azimuthal RF field component. By considering this fact along with the assumptions of constant guiding center radius and vanishing RF magnetic fields, which are very small for TE_{mn} modes near the cutoff. The equations of motion described by equations (2.25) and (2.26) can be approximated to one dimensional equation known as the adiabatic approximation. Under adiabatic approximation the equations (2.25) and (2.26) can be expressed as [Dumbrajs *et al.* (1998), Tran *et al.* (1986)]:

$$\frac{dp}{d\varsigma} = i(\Delta - 1 + |p|^2)p + iFf(\varsigma) \quad . \tag{2.28}$$

In the case of gyroklystron, due to beam-wave interaction process the bunching of electrons occurs as they drift toward the output cavity from input cavity. As these bunched electrons passes through the output cavity, a strong interaction between the electrons and the RF wave present in the cavity takes place. Thus, in a gyroklystron pre-bunching of electrons occur as they reached at the entrance of the output cavity which can be defined in terms of bunching parameter (q). The whole bunching process of the electrons in a gyroklystron can be expressed in terms of electrons phase variation (θ) and momentum variation (p) as $\theta = \theta_0 + q\sin\theta_0 - \psi$ and $p(\varsigma = \varsigma_{in}) = e^{-i\theta}$.

The gyrating electrons in gyroklystrons drift towards the output RF cavity after travelling through the one or more pre-bunching RF cavities and associated interconnecting drift tubes of the device. The drift tubes are designed such that the desired as well as competing modes are not excited, hence RF field amplitude inside the drift tube should be zero. Therefore, the equation (2.28) for drift tubes can be written as:

$$\frac{dp}{d\varsigma} = i(\Delta - 1 + |p|^2)p \quad . \tag{2.29}$$

In order to calculate efficiency of the device, electron momentum p is calculated in each RF cavities using expression (1). At the same time, the electrons phase variation θ occurring due to beam-wave interaction in the preceding cavities of

each associated interconnecting drift tubes is calculated at the end of drift tubes using expression (2.28). After this, the average of all the electrons momentum obtained at the end of the interaction length of the output cavity is taken over the initial phase angle of the electrons for calculating the transverse efficiency ($\eta_\perp$) of the device. Mathematically, it can be expressed as:

$$\eta_\perp = 1 - \int_0^{2\pi} | p(\varsigma = \varsigma_{out}) |^2 \frac{d\theta_0}{2\pi} \quad . \tag{2.30}$$

Here we have chosen $\varsigma_{in} = -\sqrt{3}\,\mu/2$ and $\varsigma_{out} = \sqrt{3}\,\mu/2$ as the normalized input and output lengths for the output cavity as they are a good approximation to actual gyroklystron output cavity.

The electronic efficiency of the gyroklystron amplifier can be simply defined as ratio of RF output energy (γ_0-γ) to the DC input electron beam energy (γ_0-1). Since, (γ_0) can be expressed in terms of beam voltage (V_b) as:

$$\gamma_0 = 1 + \frac{V_b(\text{kV})}{511} \quad . \tag{2.30a}$$

This efficiency can also be determined by calculating the average loss of electrons energy from their initial value. Therefore, electronic efficiency can be expressed in terms of electrons transverse efficiency ($\eta_\perp$) and relativistic factor (γ_0). Mathematically, using equation (2.30) and (2.30a) the electronic efficiency of the gyroklystron amplifier can be determined as:

$$\eta = \frac{\gamma_0 - \gamma}{\gamma_0 - 1} = \frac{\beta_{\perp 0}^2}{2\left(1 - \gamma_0^{-1}\right)} \eta_\perp \quad . \tag{2.31}$$

Once the electronic efficiency of the device is calculated the output power and gain of the device can be estimated as:

$$P_{out} = \eta V_b I_b \quad , \tag{2.32}$$

$$Gain = 10 \log\left[\frac{P_{out}}{P_{in}} \right] \quad , \tag{2.33}$$

where, I_b, and V_b are the beam current, and beam voltage, respectively.

2.2.1 Effect of the beam velocity spread

The electron beam velocity spread is an important aspect which should be incorporated to investigate the RF behavior of the device to have a more practical aspect. This is because during the experiments, 2% to 4% velocity spreads are always present due to which the electron beam quality degrades and as a result of this, both output power and efficiency of the device decreases. Since, the electrons emission from a real cathode is not uniform due to some of practical constraints, like, non-uniform heating of cathode, roughness in the cathode surface, and the repulsion of electrons due to space charge forces. To include these effects in the present analysis the normalized parameters described in equations (2.20a), (2.20b) and (2.20c) can be expressed in terms of the velocity dependent and independent components as [Dumbrajs *et al.* (1999)]:

$$F = C_F \beta_\perp^{s-4}, \tag{2.34a}$$

$$\mu = C_\mu \frac{\beta_\perp^2}{\beta_\parallel}, \tag{2.34b}$$

and $$\Delta = \frac{C_\Delta}{\beta_\perp^2} \quad . \tag{2.34c}$$

Here, C_F, C_μ, and C_Δ are independent to electrons transverse and axial velocity. Using the equations (2.20a), (2.20b) and (2.20c), these velocity independent normalized parameters of field, length, and detuning can be obtained as:

$$C_F = \frac{E_0}{B_0}\left(\frac{s^{s-1}}{s!2^{s-1}}\right) J_{m\pm s}(k_\perp r_b) \ , \tag{2.34d}$$

$$C_\mu = \pi \frac{L}{\lambda} \ , \tag{2.34e}$$

$$C_\Delta = 2\left(1 - s\,\omega_{c0}/\omega\right) \ . \tag{2.34f}$$

The velocity spread effects in gyroklystrons can be incorporated by considering the population of electrons having different transverse ($\beta_\perp$) and axial ($\beta_\parallel$) velocities in the above defined normalized parameters. Mathematically, the electron velocity distribution for such a population of electrons can be

approximated by a Gaussian function as were reported for gyrotrons by [Dumbrajs *et al.* (1999)]:

$$f_e(\beta_{\parallel}) = \frac{1}{\sigma\sqrt{2\pi}} \exp\left[-\frac{\left(\beta_{\parallel} - \beta_{\parallel 0}\right)^2}{2\sigma^2} \right] \tag{2.35}$$

where σ is the root mean square deviation. The full width at half maximum for axial velocity spread $\delta\beta_{\parallel}$ is taken as $2\delta\beta_{\parallel}$. Mathematically, it can be defined as:

$$\delta\beta_{\parallel} = \frac{1}{2}\left(\frac{\beta_{\parallel,\max.} - \beta_{\parallel,\min.}}{\beta_{\parallel 0}} \right) \quad . \tag{2.36}$$

Also, the axial velocity spreads are related with the root mean square deviation as:

$$\delta\beta_{\parallel} = 1.8\sqrt{2\sigma} \quad . \tag{2.37}$$

2.2.2 Linear analysis

The solutions of nonlinear equations (2.25) and (2.26) can be linearly approximated using power series method for studying the linear behavior of the gyroklystron amplifier. To perform the linear analysis, first we consider the simplest case of a two-cavity gyroklystron, i.e., only one cavity in the prebuncher and after that it can be easily extended for the multicavity gyroklystrons. Since the normalized field amplitude (F) is small, the nonlinear pendulum equations given by equation (2.25) and (2.26) are integrated analytically by expanding the normalized momentum p and electron phase θ in the small parameter F as follows [Tran *et al.* (1986)]:

$$\left.\begin{aligned} p &= p^{(0)} + p^{(1)} + \ldots \\ \theta &= \theta^{(0)} + \theta^{(1)} + \ldots. \end{aligned}\right\} \tag{2.38}$$

On inserting this expansion in equation (2.25) and (2.26) and considering the case of fundamental harmonic operation, i.e., s = 1,

$$\frac{dp^{(0)}}{d\varsigma} = 0 \tag{2.39a}$$

$$\frac{d\theta^{(0)}}{d\varsigma} = -\left(\Delta + p^{(0)^2} - 1\right) \tag{2.39b}$$

$$\frac{dp^{(1)}}{d\varsigma} = -Ff(\varsigma)\sin\theta^{(0)} \tag{2.39c}$$

$$\frac{d\theta^{(1)}}{d\varsigma} = -2p^{(0)}p^{(1)} - \frac{Ff(\varsigma)\cos\left(\theta^{(0)}\right)}{p^{(0)}} \tag{2.39d}$$

The equations (2.39a) and (2.39b) describe the undisturbed state of the electron beam (when no RF field is applied). On integrating these equations we get:

$$p^{(0)}(\varsigma) = 1 \tag{2.40a}$$

$$\theta^{(0)}(\varsigma) = \theta_0 + \Delta(\varsigma_{in} - \varsigma) = \theta_0 - \Delta\varsigma \tag{2.40b}$$

where θ_0 is uniformly distributed all over the phase [0, 2π]. Now equation (2.39c) which describes the electron momentum modulation by the RF field is integrated using field profile equation (2.28) and equation (2.40b). This gives the electron momentum at the output of the first cavity approximated up to the first order in F as:

$$p_1(\varsigma_{out}) = p^{(0)}(\varsigma_{out}) + p^{(1)}(\varsigma_{out}) = 1 - \frac{\sqrt{\pi}}{2}F_1\mu_1 G(x)\sin\theta_0 \tag{2.41}$$

where the function G is defined by

$$G(x) = \frac{2}{\sqrt{\pi}}\int_0^{\sqrt{3}} e^{-t^2}\cos(2xt)\,dt \approx e^{-x^2} \quad , \tag{2.42}$$

and $x = \mu\Delta/4$.

Similarly, equation (2.39d) which describes the bunching of the electron phase angles is solved and the obtained results of this equation are added to equation (2.40b) to get the electron phase angles at the output of the first cavity is given by:

$$\theta_1(\varsigma_{out}) = \theta_0 - \frac{\sqrt{3}}{2}\mu_1\Delta + \frac{\sqrt{\pi}}{2}F_1\mu_1 e^{-x^2}\left\{\sqrt{3}\mu_1\sin\theta_0 + \mu_1 x\cos\theta_0 - \cos\theta_0\right\}. \tag{2.43}$$

After the first cavity, drift section is there where momentum p remains constant (since no RF field is excited, i.e., F = 0) and due to inertial bunching mechanism bunched phase angles θ will evolve in drift tube as:

$$\frac{d\theta}{d\varsigma} = -\Delta + \sqrt{\pi}F_1\mu_1 e^{-x_1^2}\sin\theta_0 \quad . \tag{2.44}$$

The bunched phase angles at the end of the drift section is obtained by solving above equation with the initial condition specified by equation (2.43):

$$\theta_b = \theta_0 - \left(\frac{\sqrt{3}}{2} \mu_1 \Delta_1 + \mu_d \Delta_d \right) + q \sin \theta_0 \quad , \tag{2.45}$$

where μ_d is the drift length and q is defined as the bunching parameter and is given by:

$$q = \sqrt{\pi} F_1 \mu_1 e^{-x_1^2} \left(\frac{\sqrt{3}}{2} \mu_1 + \mu_d \right) \quad . \tag{2.46}$$

As a result, the electron phase angles, at the input of the second cavity can be parameterized by the bunching parameter q and the constant phase ψ which is the phase difference between the cavities and the electron rotational drift, as:

$$\theta_{0,2} = \theta_0 + q \sin \theta_0 - \psi \tag{2.47}$$

$$\psi = (\sqrt{3}/2) \mu_1 \Delta_1 + \mu_d \Delta_d \quad . \tag{2.48}$$

Again, on solving the pendulum equations up to the first order in F_1 and F_2, the transverse momentum at the output of the second cavity can be easily calculated as:

$$p_2(\varsigma_{out}) = 1 - \frac{\sqrt{\pi}}{2} F_1 \mu_1 e^{-x_1^2} \sin \theta_0 - \frac{\sqrt{\pi}}{2} F_2 \mu_2 e^{-x_2^2} \sin \left[\theta_{0,2} - \frac{\sqrt{3}}{2} \mu_2 \Delta_2 \right] \quad . \tag{2.49}$$

Using equation (2.49), one can calculate the small-signal efficiency of the device as the orbital efficiency which is necessary for calculating the electronic efficiency of a gyroklystron amplifier is obtained by performing an average over the initial phase angles θ_0 and mathematically it can be expressed as:

$$\eta_\perp^{lin} = 1 - \left\langle p_2^2 \left(\varsigma_{out} \right) \right\rangle_{\theta_0} \quad . \tag{2.50}$$

In the output cavity of the gyroklystron, the range of integration is taken as $-\sqrt{3}\mu/2 \leq \varsigma \leq \sqrt{3}\mu/2$. By using equations (2.47), (2.49), and (2.50), we can obtain the relation for the electronic efficiency as:

$$\eta = \sqrt{\pi}/2 \, F_2 \mu_2 e^{-x_2^2} J_1(q) \sin \left(\psi + (\sqrt{3}/2) \mu_2 \Delta_2 \right) \left(\frac{\beta_{\perp 0}^2}{\left(1 - \gamma_0^{-1} \right)} \right) \quad , \tag{2.51}$$

where F_2 is the normalized field amplitude induced in the second cavity by the phase-bunched and is given by [Gold *et al.* 1990]:

$$F_2 = \sqrt{\pi} I_2 \mu_2 e^{-(\mu_2 \Delta_2/4)^2} J_1(q) \left(\sin\psi + \frac{\mu_2^2 \Delta_2 / 4 - 1}{(\sqrt{3}/2)\mu_1 + \mu_d} \cos\psi \right) \quad . \tag{2.52}$$

Here, I_2 is the normalized beam current defined as:

$$I_2 = \left(\frac{2}{\pi^5} \right)^{1/2} \frac{I_b Q e}{c^3 m_e \varepsilon_0} \frac{\beta_{\perp 0}^{-4}}{\gamma_0} \frac{\lambda}{L_2} \frac{J^2{}_{m\pm s}(k_\perp r_b)}{(\upsilon_{mp}{}^2 - m^2) J_m{}^2(\upsilon_{mp})} \quad . \tag{2.53}$$

Here, I_b is the beam current in amperes, Q is the total quality factor of cavity, and L_2 is the length of the output cavity. If I_2 and F_2 are known, the transverse efficiency can also be obtained by using power balance equation as:

$$\eta_\perp I_2 = F_2^2 \quad . \tag{2.54}$$

The analysis discussed above generalizes to an N-cavity gyroklystron as follows:

$$p_{out,j} = 1 - \frac{\sqrt{\pi}}{2} \sum_{k=1}^{j} F_k \mu_k e^{-x_k^2} \sin\theta_{0,k} \tag{2.55}$$

$$\theta_{c,j+1} = \theta_{c,j} + \hat{\mu}_{d,\mathrm{j}} \sum_{k=1}^{j} \frac{q_k}{\hat{\mu}_{d,k}} \sin\theta_{0,k} - \hat{\psi}_j \tag{2.56}$$

where, j = 1 to N-1, $p_{out,j}$, is the normalized momentum at the output of the j^{th} cavity, $\theta_{c,j+1}$ is the phase angles at the mid-plane of the $(j+1)^{\text{th}}$ cavity and

$$\hat{\mu}_{d,\mathrm{j}} = \frac{\sqrt{3}}{2} \mu_j + \mu_{d,j} \quad , \tag{2.57a}$$

$$q_j = \sqrt{\pi} F_j \mu_j \hat{\mu}_{d,\mathrm{j}} e^{-x_j^2} \quad , \tag{2.57b}$$

and

$$\hat{\psi}_j = \frac{\sqrt{3}}{2} \mu_j \Delta_j + \mu_{d,j} \Delta_{d,j} + \frac{\sqrt{3}}{2} \mu_{j+1} \Delta_{j+1} + (\psi_{j+1} - \psi_j) \quad . \tag{2.57c}$$

2.3 Results and Discussion

The gyroklystron analyses developed above are used to examine the RF behavior of the amplifier; the numerical codes have been developed for this purpose. These codes are further used for the design and analysis of the gyroklystron in the subsequent chapters. In the present analyses, the differential equations are solved using fourth order Runge-kutta method. In the numerical integration of the coupled equations (2.25) and (2.26) of the single-mode analysis, 64 macro-electrons are used, with zero initial energy and equally distributed in

initial phase. The limit of integration is taken as $-\sqrt{3}\mu/2 < \varsigma < \sqrt{3}\mu/2$ which corresponds to *exp*(-3) power points of axial field profile, which is a good approximation for the resonant cavities, which are used as the RF interaction structure in gyroklystrons [Fliflet *et al*. (1982)]. Each macro electron represents a group of electrons starting with similar energy and phase distribution. For the accuracy, number of electrons should be increased. For the 64 number of particles, accuracy is found to be sufficient enough. All the electrons are assigned the initial transverse and longitudinal energy based on the calculation done from the beam voltage (V_b) and the velocity pitch factor (α). The electrons are uniformly distributed over the interval [0, 2π].

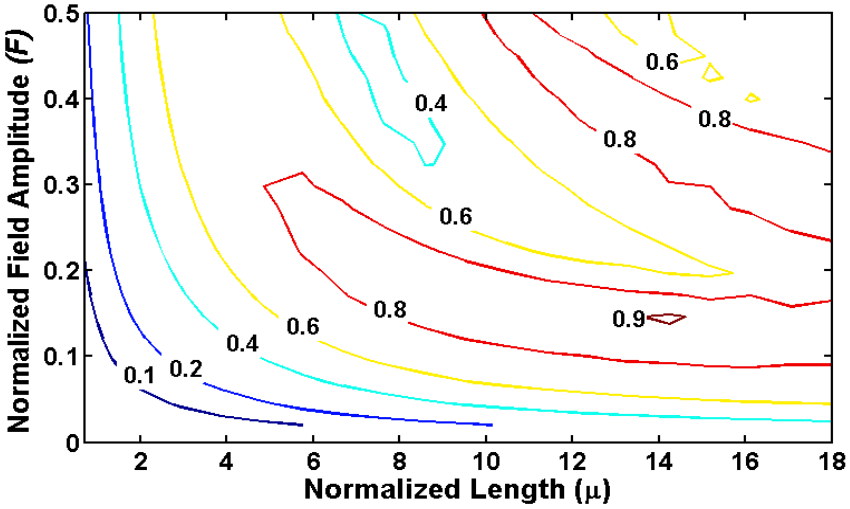

Fig. 2.2 Contour plot of orbital efficiency ($\eta_\perp$) as a function of normalized field amplitude (F) and normalized length (μ).

2.3.1 Efficiency contours

The single-mode analysis described in the preceding section 2.2 is used to calculate the momentum and phase of the electrons, contour plots of transverse efficiency, output power. The nonlinear pendulum equations (2.25)-(2.26) are solved using fourth order Runge-Kutta algorithm with Gaussian axial field profile. Consequently, the contour plots of the efficiency ($\eta_\perp$) in F-μ and I-μ space is obtained. The contour plot $\eta_\perp(F,\mu)$ is used for the optimization of the gyroklystron design. Since, all the relevant design parameters such as wall loading, beam thickness effect, and voltage depression can be expressed in terms

of F and μ [Kreischer *et al*. (1985), Tran *et al.* 1986]. The $\eta_{\perp}(I,\mu)$ contour plot can be used to determine the efficiencies for known value of beam current.

An efficiency contour plot of a gyroklystron amplifier in F-μ space is shown in Fig. 2.2 for the fundamental harmonic operation. In the figure, for each value of F and μ, the optimum Δ has been estimated corresponding to the maximum efficiency. The maximum transverse efficiency is obtained 90%, corresponding to F and μ as 0.145 and 15.5, respectively. This figure provides qualitative information about the performance of the gyroklystron in terms of the work done on the electron bunch with the variation of normalized field amplitude (F) and normalized interaction length (μ). At the lower value of F and μ the efficiency value is small, which reveals the little work done on the electron beam. With the increase in value of these two parameters, the efficiency increases, and at a certain point, it reaches to its maximum. Further increasing the value of F and μ, the efficiency value is reduced, which means that electron beam starts gaining the energy from the RF wave. In this plot, several high efficiency regions are obtained but the gyroklystron design is preferred in the lowest value of the F and μ region due to some physical and technological constraints such as start oscillation current, beam spreading and space charge effects.

Further, in order to study the evolution of electron bunching on orbital efficiency $\eta_{\perp}$, the momentum of the electrons versus axial distance has been plotted for different values of device parameters. In Fig. 2.3, the momentum of electrons has been plotted against the axial position of the output RF cavity for a set of gyroklystron parameters corresponding to the optimum bunching condition, i.e., field amplitude (F) = 0.145, length (μ) = 15.5, detuning parameter (Δ) = 0.538, bunching parameter (q) = 3.17, and RF phase $\psi = 0.84\pi$, necessary for maximum efficiency. Under this optimum condition, the electron bunches give up their maximum energy to the RF field. It can be seen from Fig. 2.3, that towards the output end of the interaction length, a large number of electrons are in the lower momentum state and only few of them are in a higher momentum side. The corresponding phase bunching of the electrons in axial direction is shown in Fig. 2.4. The maximum axial bunching occurs nearly at the middle of the output

cavity where RF field is maximum in the cavity as shown in Fig. 2.5. This shows that a strong beam-wave interaction process takes place at the center of the output cavity.

The Fig. 2.6(a) has been plotted for the same optimized parameters, only the bunching parameter q value has been increased to 4.5 in order to see the effect of over bunching. This results in degradation of the efficiency from 89% to 55% due to the presence of more electrons in the higher momentum side at the output end as shown in the Fig. 2.6(a). The efficiency further decreases, when we reduce the frequency detuning parameter Δ from its optimized value as shown in Fig. 2.6(b). This happens due to the presence of most of the electrons in a higher momentum side, resulting in poor bunching and hence less efficiency as the electrons energy is very less perturbed by the RF from their initial value due to weak beam-wave interaction process.

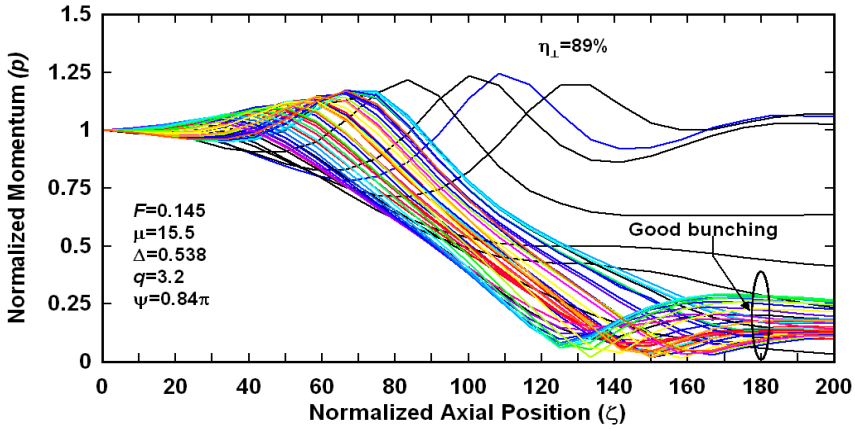

Fig. 2.3 Normalized momentum as a function of normalized interaction length for optimum bunching condition.

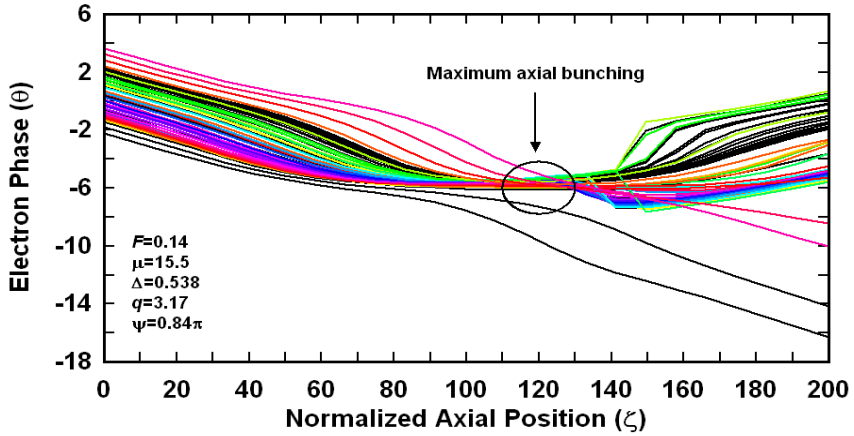

Fig. 2.4 Electrons phase bunching along the normalized distance .

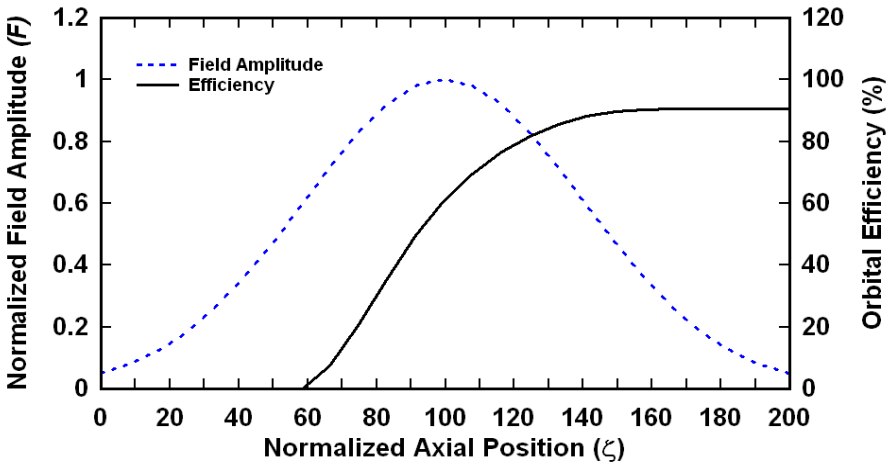

Fig. 2.5 Normalized field amplitude and transverse efficiency as a function of normalized distance.

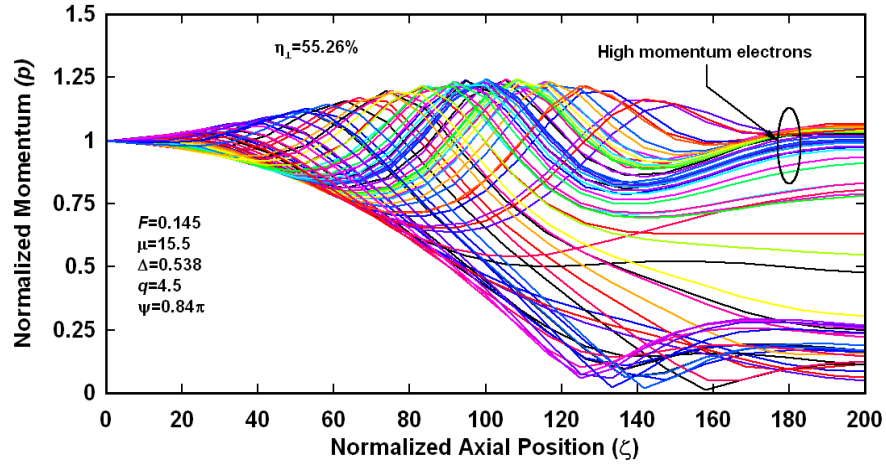

(a)

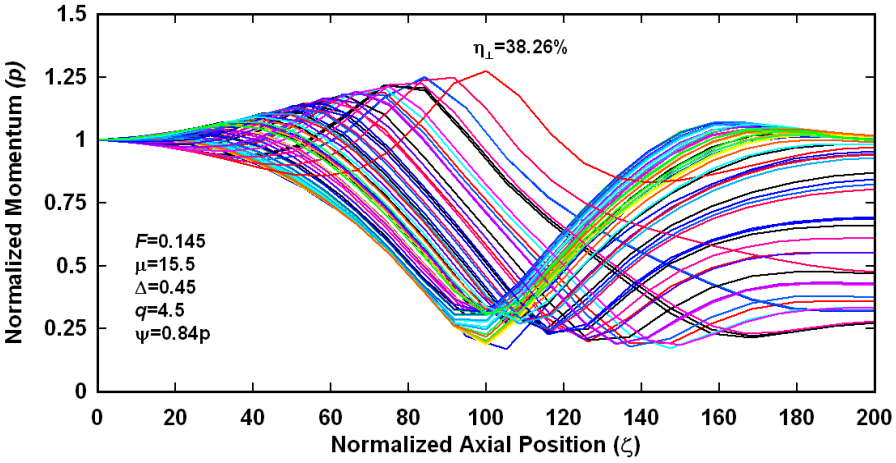

(b)

Fig. 2.6 Normalized momentum versus normalized distance plots for a set of gyroklystron parameters (a) over bunching condition, and (b) variation in detuning parameter from optimal bunching.

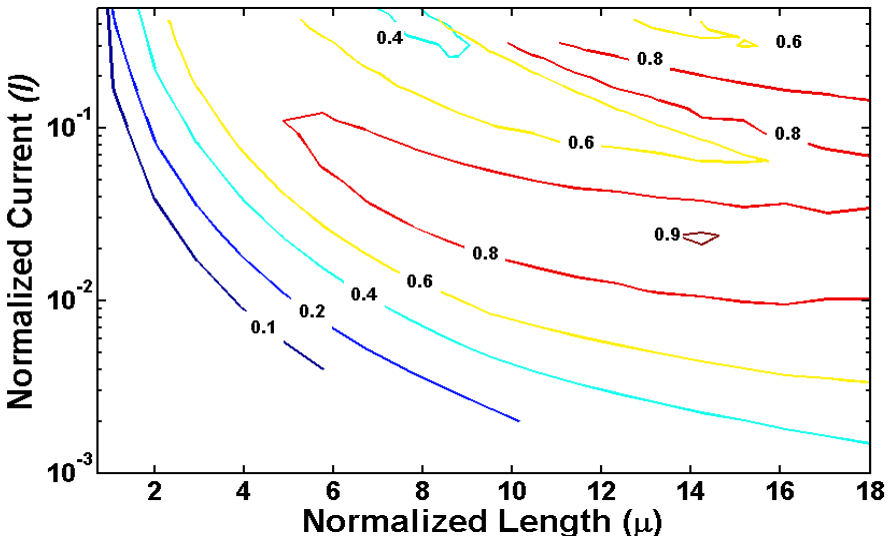

Fig. 2.7 Contour plot of orbital efficiency as a function of normalized beam current and normalized length.

The contour plots of the efficiency in I-μ space corresponding to F-μ space optimized with Δ, q and ψ is shown in Fig. 2.7, which is obtained using energy balance equation. The $\eta_{\perp}(I,\mu)$ contour plot is helpful in deciding the value of the beam current for the optimum efficiency. It must be noticed that these plots are quite general and can be applied to design the gyroklystron of any value of frequency and output power.

2.3.2 Numerical Benchmarking

The generalized linear and nonlinear analyses discussed in the preceding section 2.2 are further exploited to observe the gyroklystron amplifiers behavior with the aid of computer friendly numerical code. To validate the developed analytical model, Ka-band two-cavity and four-cavity gyroklystron amplifiers experiments reported in the literature have been selected [Choi *et al.* (1998), Garven *et al.* (2000)]. This performance estimation has been carried for the numerical benchmarking the code, so that they can be successfully implemented for the design and analysis of the gyroklystron amplifier in the subsequent chapters. The flowchart in Fig. 2.8 illustrates the step by step procedure followed for the output performance realization of a gyroklystron amplifier.

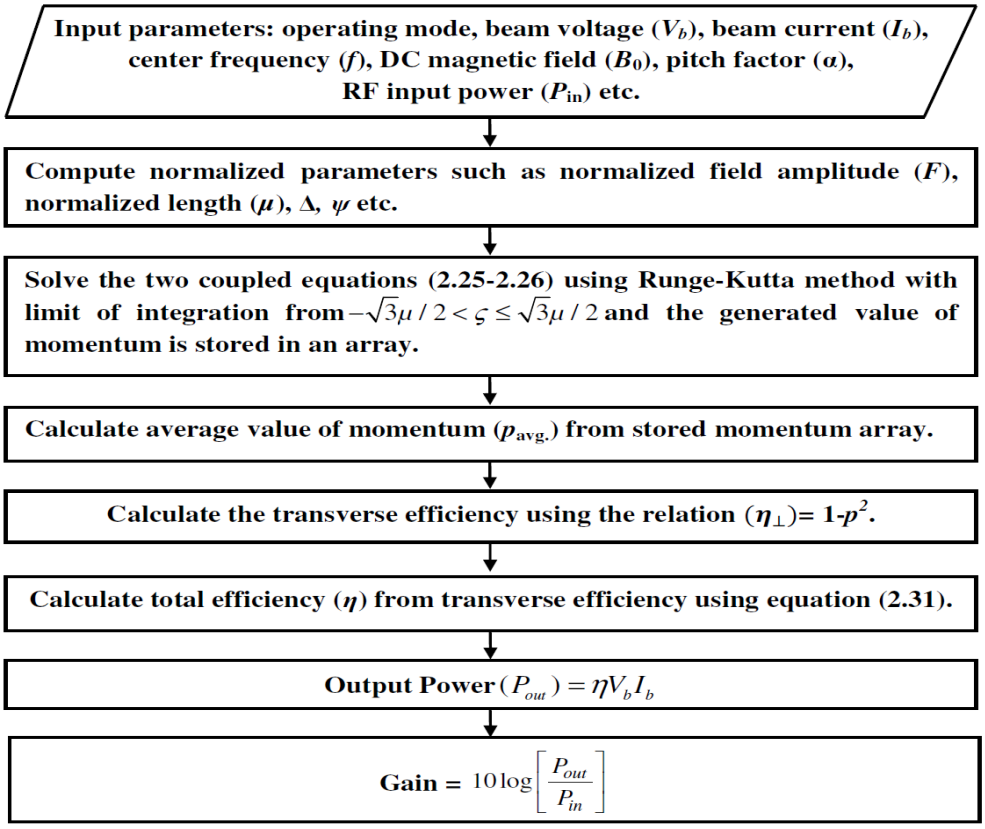

Fig. 2.8 Flow chart for the performance estimation of a gyroklystron amplifier.

Table 2.1 Design specifications for 35 GHz, 200 kW two-cavity gyroklystron amplifier [Choi *et al.* (1998)].

Parameters	Specifications
Operating Mode	***TE*$_{01}$**
Beam Voltage (V_b)	**70 kV**
Beam Current (I_b)	**8.2 A**
Velocity Pitch Factor (α)	**1.43**
Center Frequency (f)	**34.95 GHz**
DC Magnetic Field (B_0)	**1.31 T**
Input Cavity Length	**12.85 mm**
Output Cavity Length	**23.56 mm**
Input Cavity Radius	**5.6 mm**
Output Cavity Radius	**5.35 mm**
Drift Tube Length	**14.57 mm**
Drift Tube Radius	**4.1 mm**

2.3.2b Two-cavity gyroklystron amplifier

The analysis of 35 GHz, 200 kW fundamental harmonic two-cavity gyroklystron with all the cavities operating in the TE_{01} mode has been carried out using the approach developed above. Table 2.1 shows the design specifications taken for analysis of 35 GHz, 200 kW two-cavity gyroklystron.

The operating point of the present gyroklystron has been chosen with the help of the efficiency contour corresponding to its normalized output cavity length. The electronic efficiency of the device under consideration is calculated by using the linear and nonlinear theory.

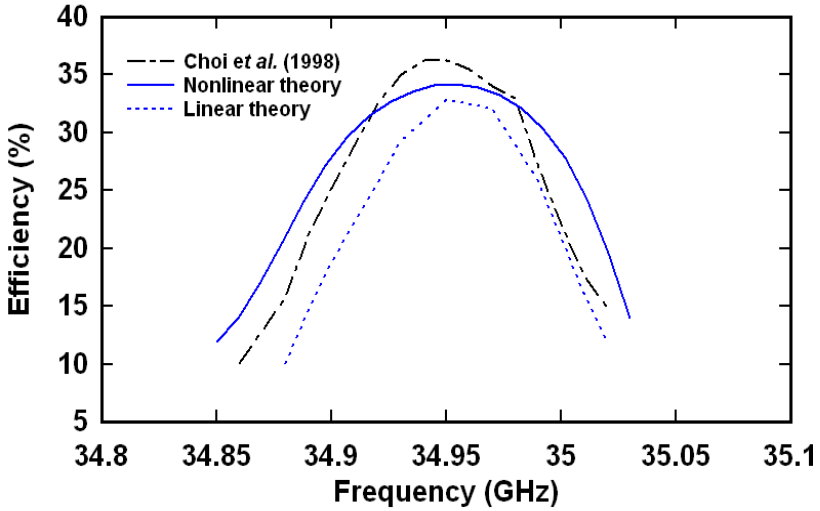

Fig. 2.9 Efficiency as a function of frequency.

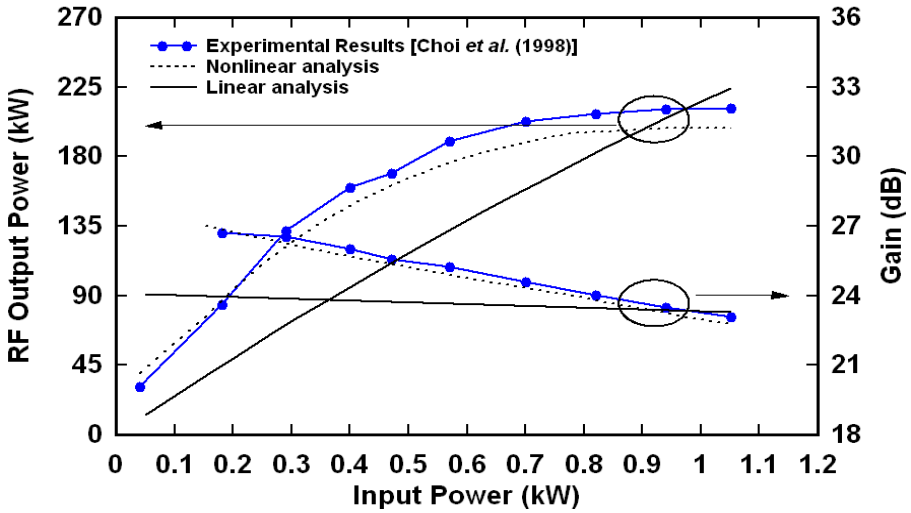

Fig. 2.10 RF output power and gain as a function of input power.

Figure 2.9 shows the comparison of the reported experimental results with the analytically obtained results from the linear and nonlinear analysis for the variation of output power with drive frequency. It is clear from Fig. 2.9 that the present gyroklystron amplifier achieves highest efficiency at center frequency 34.95 GHz. The electronic efficiency corresponding to the center frequency 34.95 GHz as estimated by the linear theory is 32.8%, and from nonlinear analysis is 35%. The experimental reported efficiency of this device is around 36%.

Figure 2.10 shows the peak output power and gain as a function of input power calculated analytically using linear and nonlinear theories. As seen from figure, the output power reaches the saturated value of 200 kW at 922 W drive power corresponding to 23.36 dB gain. Furthermore, the analytical results obtained here are validated against the experimental results reported in the literature. The results obtained here from nonlinear analysis are found to be in good agreement with the reported experimental values, whereas the deviation of linear theory results can be explained on account of its limitation not to consider the nonlinear saturation effects.

Table 2.2 Design specifications for 35 GHz, 200 kW four-cavity gyroklystron amplifier [Garven *et al.* (2000)]

Particulars	**Specifications**
Mode	TE_{01}
Beam Voltage (V_b)	**72 kV**
Beam Current (I_b)	**9.6 A**
Velocity Ratio (α)	**1.36**
DC Magnetic Field (B_0)	**1.335 T**
Input Cavity Length	**12.88 mm**
Second Cavity Length	**14.59 mm**
Third Cavity Length	**14.59 mm**
Output Cavity Length	**23.58 mm**
Drift Tube Length	**14.59 mm**
Quality Factor (Input Cavity)	**188**
Quality Factor (Second Cavity)	**200**
Quality Factor (Third Cavity)	**200**
Quality Factor (Output Cavity)	**170**

2.3.2b Four-cavity gyroklystron amplifier

Like the conventional klystrons, the two-cavity gyroklystron serves as the basic model for the gyroklystron amplifier. However, it is not so practical useful. Since, its gain is limited due to the limited beam-wave interaction process. The typical power gain of a two-cavity gyroklystron amplifier is about 20 dB. In order to achieve a higher gain, the bunching process in a gyroklystron amplifier needs to be enhanced. Addition of more bunching cavities in between the first cavity and the output cavity strengthens the bunching process, that produces an increase in the energy available at the output, and hence the overall gain of the device increases. The overall efficiency of the tube is also improved to a lesser extent. Moreover, one can achieve higher bandwidth in a multicavity gyroklystron as compared to two-cavity gyroklystron by stagger tuning the various cavities to slightly different frequencies [Choi (1998), Nusinovich *et al.* (1997)]. Keeping these points into consideration, and to make the present study more useful for a practical device, the analysis of a Ka-band, four-cavity gyroklystron amplifier is implemented.

The analysis of 35 GHz, 200 kW fundamental harmonic four-cavity gyroklystron with all the cavities operating in the TE_{01} mode has been presented using linear and nonlinear theories. Table 2.2 shows the design specifications taken for analysis of 35 GHz, 200 kW four-cavity gyroklystron amplifier.

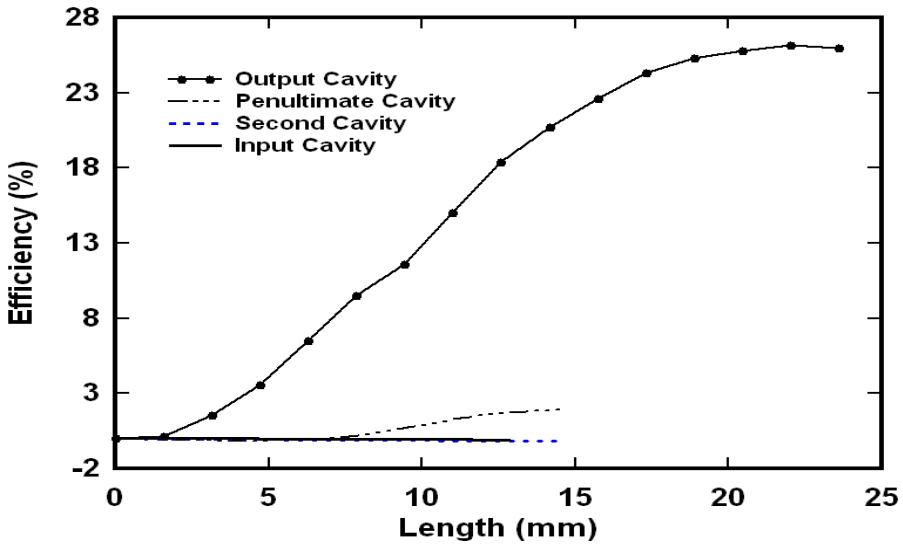

Fig. 2.11 Electronic efficiency variation in each cavity as a function of length.

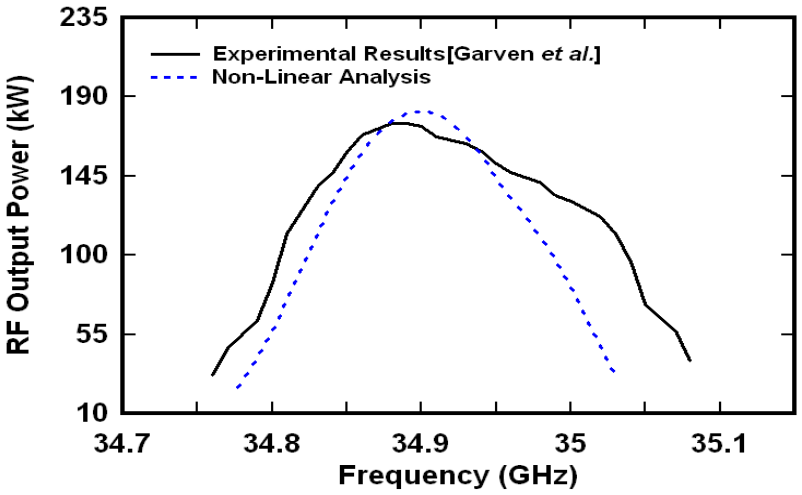

Fig. 2.12 RF output power as a function of frequency.

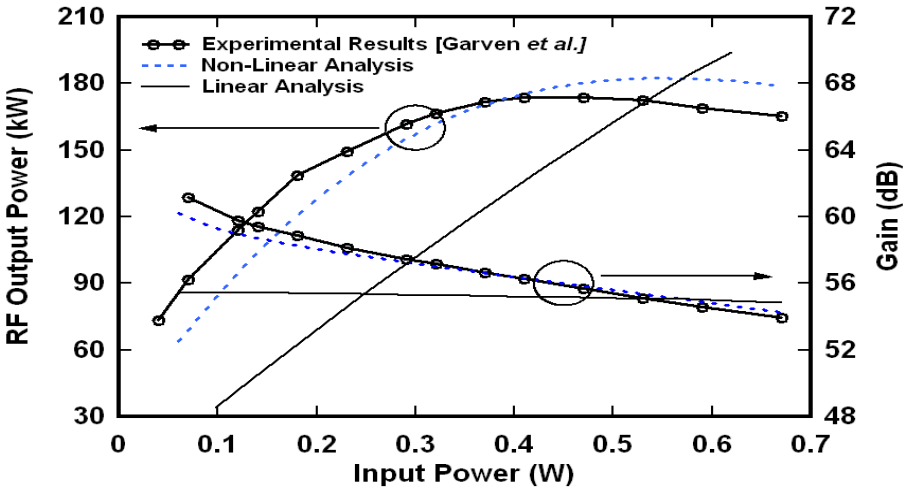

Fig. 2.13 Output power and gain as function of input power.

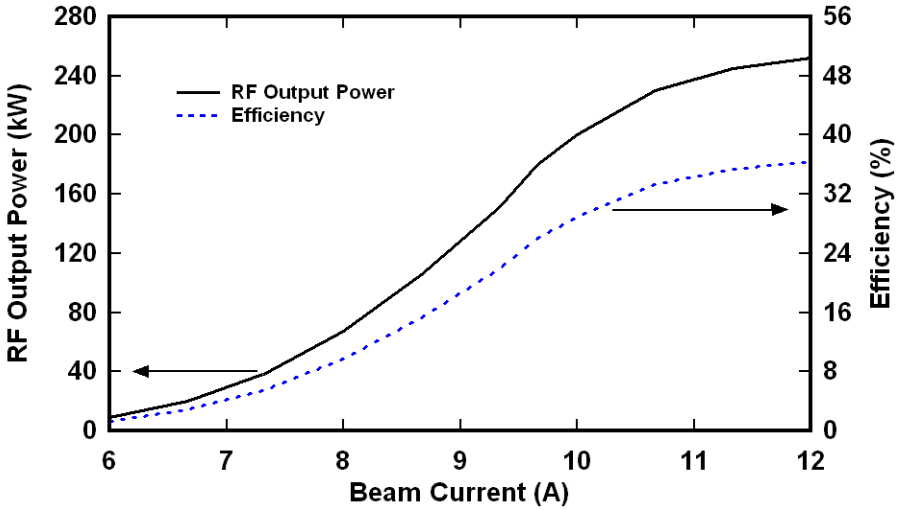

Fig. 2.14 Output power and efficiency variation with beam current.

The electronic efficiency of the device which is defined as the conversion of DC beam power to RF output power is calculated using equation (2.31). The electronic efficiency in each cavity is shown in Fig. 2.11. It can be seen from Fig. 2.11 that as the electrons move from input cavity to output cavity the efficiency in each cavity increases. Also, one can see that the efficiency in input cavity and second cavity is quite small. This is because energy exchange between the RF and the electron beam is very small in these cavities due to net energy is gained by the electrons for bunching process. The maximum efficiency is obtained at the output cavity due to the strong beam wave interaction occurring between the azimuthally bunched electron beam and the RF induced by these electrons in the output cavity. The resultant electronic efficiency is about 26% and the corresponding output power is around 180 kW. Figure 2.12, shows the comparison of the reported experimental results with the analytically obtained results for the variation of output power with drive frequency. It is clear from Fig. 2.12 that the present gyroklystron amplifier achieved 180 kW peak output power at center frequency 34.9 GHz with a -3 dB bandwidth of 202 MHz (0.58%). It can be seen from the Fig. 2.12, the analytical results obtained here are in good agreement with the reported experimental results within ± 5%. Fig. 2.13 shows the peak output power and gain as a function of input power. As seen from figure, the output power reaches the saturated value of 180 kW at 0.43 W drive power corresponding to 56 dB gain in case of nonlinear theory and 142 kW with 55 dB gain from linear theory. The results obtained from nonlinear analysis are in agreement with the reported experimental results within ~5%.

2.3.3. Sensitivity Analysis

The sensitivity analysis of the gyroklystron amplifier is carried out in detail by studying its parametric variation with different parameters with the help of four-cavity gyroklystron selected in the previous section. The output power and efficiency variation has been observed with respect to beam current, quality factor and electron beam velocity ratio.

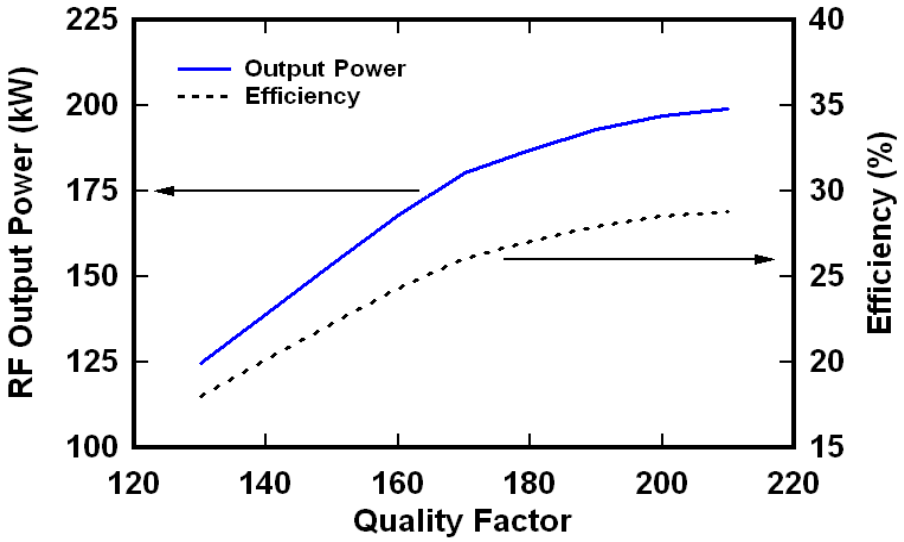

Fig. 2.15 Output power and efficiency variation with quality factor.

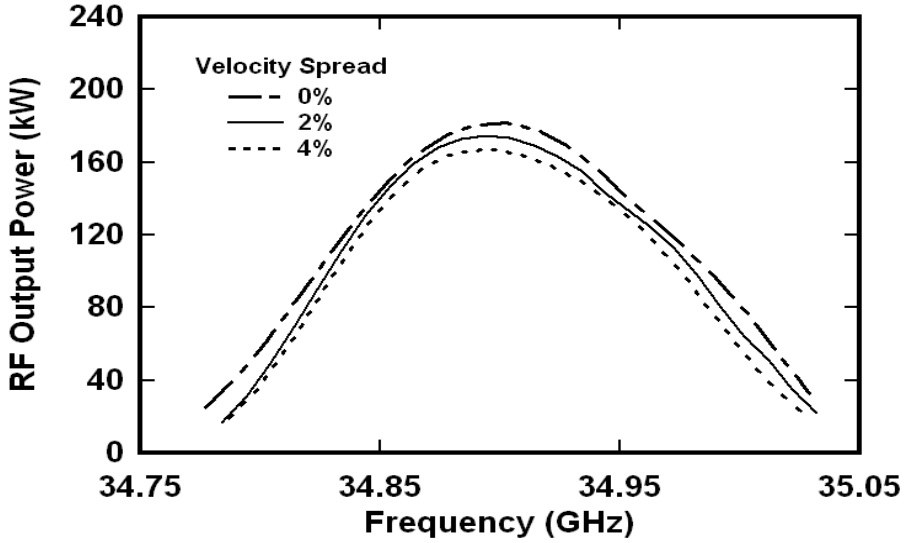

Fig. 2.16 RF output power variation with frequency for different velocity spreads.

The output power and efficiency increases as the beam current increases, which is due to the operation of the device near the start oscillation current (Fig. 2.14). The Fig. 2.15 shows the variation of output power and efficiency as a function of the quality factor of the output cavity. The peak output power about 200 kW has been obtained around quality factor 210. However, the quality factor of the output cavity is chosen 170 for the stable operation of the device corresponding to peak output power 180 kW in order to avoid the undesired oscillation which occurs due to the operation of the device very near to start

oscillation current. The electron beam velocity spread plays a vital role in power growth mechanism inside the cavity. In Fig. 2.16, the effect of electron beam velocity spread on the output power and bandwidth is analyzed. The output power and bandwidth decrease as the beam velocity spread increases. This happens because some of the electrons have lower energies and hence transfer lesser amount of energy to the RF. For an ideal beam with no velocity spread, the peak output power is 180 kW and for a beam with 4% velocity spread, the peak output power is 165 kW at 34.9 GHz. Accordingly, the 3 dB bandwidth of the device drops from 0.58% to 0.46%.

2.3 Conclusion

For the analysis of a gyroklystron amplifier, both small signal and large signal analyses are in vogue. Small signal analysis based on the linear theory is used to study the device behavior in the linear regime. On the other hand, the large signal analysis based on the nonlinear theory is used to predict output power, efficiency, saturated gain, and phenomenon of electron cross-over and debunching thereby providing better understanding of the beam-wave interaction and saturation mechanisms. A self-consistent nonlinear signal formulation for the gyroklystron has been developed considering electron velocity spread effects to study the beam-wave interaction behavior of a gyroklystron amplifier under the time independent single mode consideration.

The electron beam velocity spread always present practical device because of the non-uniform electrons emission from a real cathode due to practical constraints, like, non-uniform heating of cathode, cathode surface roughness, and electrons repulsions due to space charge. 2 to 4% electron velocity spreads are usually found in the practical devices and this degrades the tube performance, both RF output power and efficiency. The nonlinear analysis is modified to include this effect by making the normalized parameters: field amplitude, momentum and electron phase terms velocity dependent.

Gyroklystron efficiency is optimized by optimally selecting the field amplitude, length and detuning parameters as well as value of the beam current.

The existing manual method of optimizing efficiency through the contour plots of the efficiency has been made automatic logical loop controlled.

Taking resort of the reported experimental work, the performance of typical 35 GHz, cylindrical two-cavity and four-cavity gyroklystron amplifiers operating at the TE_{01} mode, using the analytical approach developed here, has been investigated as well as validated. The results obtained through the nonlinear analytical model developed here have been found in agreement of ~5% with those of the reported experimental values.

The effects of the various device parameters, such as, variations in the beam current, quality factor, beam voltage, and velocity spread on the device electronic efficiency, bandwidth and RF output power are explored and discussed. This sensitivity studies will help this device developer to analyze their device under practical conditions.

The analytical results obtained by the large signal analysis developed in the present chapter will also be validated with the PIC simulation values obtained using available 3D commercial software MAGIC in the next chapter, Chapter 3. After validating our large signal analysis through PIC simulations, the studies will be extended further in the subsequent chapters for exploring the design and performance improvements techniques of the gyroklystron amplifiers.